Neutron emission from products of strongly damped reactions $^{58}Ni + ^{165}Ho$ at 930 MeV

G. A. Petitt, C. Butler, and V. Penumetcha
Georgia State University, Atlanta, Georgia 30303

T. C. Awes, J. R. Beene, R. L. Ferguson, F. E. Obenshain, F. Plasil, and G. R. Young
Oak Ridge National Laboratory, Oak Ridge, Tennessee 37831

S. P. Sorensen
University of Tennessee, Knoxville, Tennessee 37996
and Oak Ridge National Laboratory, Oak Ridge, Tennessee 37831

(Received 2 March 1989)

Neutron time-of-flight spectra have been measured for emission from products of reactions between ^{58}Ni and ^{165}Ho at a bombarding energy of 930 MeV. Neutrons were detected in coincidence with projectilelike fragments from strongly damped reactions using a heavy ion ΔE-E telescope which permitted the total kinetic energy loss to be extracted for each event. The neutron spectra were separated into 25-MeV-wide total kinetic energy loss bins over the total kinetic energy loss range from 0 to 450 MeV. Moving source fits were made to the neutron spectra to determine emission temperatures, multiplicities, velocities, and angles for the projectilelike fragment, targetlike fragment, and nonequilibrium emission sources as a function of the total kinetic energy loss. The extracted temperature of the projectlike fragment is found to be larger than that of the targetlike fragment source at all total kinetic energy losses, approaching that of the targetlike fragment only at the largest total kinetic energy losses. The results suggest an equal division of the available excitation energy at small total kinetic energy loss with a thermal energy division occurring only at the largest total kinetic energy losses. The velocity of the nonequilibrium source is found to remain constant at approximately one-half of the beam velocity independent of the final projectlike fragment velocity. This result supports models of nonequilibrium emission in which nucleon emission is isotropic in the nucleon-nucleon center-of-mass system as opposed to models in which the nonequilibrium emission occurs isotropically from the heavy fragments along their reaction trajectories.

I. INTRODUCTION

At energies above 10 MeV/nucleon nonequilibrium nucleon emission is observed to become a significant aspect of heavy-ion-induced reactions. A number of experiments have been reported recently in which nonequilibrium emission has been studied under various controlled conditions.[1-17] Multiplicities of nonequilibrium neutrons as high as three are observed in coincidence with evaporation residues at high excitation energy.[14] The nonequilibrium emission has been parametrized with some success in terms of emission from a source moving in the beam direction. The source velocities that are extracted from fits to the spectra are usually about one-half the beam velocity or less. This simple parametrization has not been completely successful in describing all of the data, however. For example, a preferential nonequilibrium emission in the reaction plane has been observed in several cases.[8,17,18] This effect is most pronounced for neutrons in coincidence with fission fragments and seems to result from the effects of high angular momentum of the emitting system. In the case of neutrons emitted in coincidence with projectilelike fragments (PLF) in inelastic scattering reactions, the angular distribution of the nonequilibrium emission is not necessarily symmetric about the beam direction. In one case it was found to be peaked on the opposite side of the beam from the direction of the coincident PLF;[4] in another case it was found to be peaked on the opposite side of the beam from the PLF for quasielastic events but symmetric about the beam direction for deep-inelastic events;[3] and in a third case, it was found to be peaked on the same side of the beam as the coincident PLF for quasielastic events but on the opposite side of the beam for deep-inelastic events.[19]

A number of models have been developed to explain the mechanism by which these nonequilibrium particles are emitted. These models may be divided into two basic categories. In one group emission is assumed to occur from an overlap of roughly equal contributions of target and projectile nucleons, with the prediction that the nonequilibrium nucleons are emitted approximately isotropically from a rest frame moving at about one-half the beam velocity, independent of the final velocity of the PLF.[20-23] This result is characteristic of hot-spot models[20,21] that assume the formation of an evaporation source consisting of roughly equal nucleon contributions from the target and projectile. It is also characteristic of direct knockout models[20,22] that assume the nucleon emission to result from quasifree nucleon-nucleon scattering. Finally, it is characteristic of a recently presented

transport model in which projectile nucleons are pictured as scattering from individual target nucleons after traversing a window in the neck joining the target and projectile during their collision.[23] In the second group of models[24–28] the nonequilibrium nucleons are assumed to be emitted in the respective rest frames of the reaction partners along their reaction trajectories. As a result these models will predict that the nonequilibrium emission from the PLF appears to occur from a frame which moves with a velocity between that of the incident beam velocity and the minimum velocity of the projectile during contact. This result is expected for models which assume that the emission from the projectile is due to the interaction of the projectile with the time-dependent mean field of the target such as the dissipative diabatic dynamics model,[24] the simplest form of the Fermi-jet-type models,[25,26] and time-dependent Hartree-Fock (TDHF) models.[27,28]

It is difficult to place the exciton models[29–32] in either of these categories. Two of the models can only be compared with angle-integrated spectra so that there is no information about source velocity.[29–31] The third model permits comparison with angular distributions but it is not clear what range of course velocities is consistent with the predictions of the model.[32]

Predictions of angular distributions and multiplicities of nonequilibrium light particles from specific reactions have been made recently using several of these models and compared with experimental results. Both classes of models have had about equal success in explaining the data. For example, Awes *et al.*[20] compared their inclusive measurements with an exciton model, a hot-spot model, and a knockout model, and other authors have compared the same results with a second exciton model[32] and with a nucleon-nucleon interaction model,[22] all with some success.

In light of the uncertainty about the basic mechanism underlying nonequilibrium emission, it may be helpful to make a direct comparison between source velocities determined from fits to experimental spectra and model predictions. In the experiment reported here we have attempted to observe the nonequilibrium neutron emission and determine the nonequilibrium source velocity as a function of total kinetic energy (TKE) loss and final PLF velocity for comparison with the predictions of the TDHF model of Umar *et al.*[27,28] and hence, as a means to distinguish between these two classes of models.

II. EXPERIMENT

The experiment was performed at the Holifield Heavy Ion Research Facility of the Oak Ridge National Laboratory using coupled operation of the tandem electrostatic accelerator and cyclotron. A 930-MeV pulsed beam of ^{58}Ni ions was used to bombard a ^{165}Ho metal target of 1 mg/cm^2 thickness. The target was mounted at the center of an 80-cm diameter spherical aluminum target chamber of 3-mm wall thickness. A heavy-ion detector telescope, which was comprised of a gas ionization chamber (ΔE) backed by a position sensitive silicon (E) detector, was used to measure the energy, charge, and angle of PLF fragments. It was located inside the target chamber and was used as the primary event trigger. This detector subtended an angular range from 11.5° to 23.5°, which included the grazing angle (15°), and covered a solid angle of 9.3 msr. The position signal was calibrated by measuring alphas from a source located in the target position through a slotted mask placed in front of the detector. The angular resolution was approximately 0.5°.

Neutrons were measured in coincidence with PLF's in an array of liquid scintillator detectors located outside the target chamber. Ten neutron detectors had scintillator cells of 12-cm diameter and 5-cm thickness mounted on 12-cm diameter photomultiplier tubes. Two position-sensitive detectors were constructed of 1-m-long quartz tubes which had rectangular cross sections of 12-cm height and 6-cm thickness. The scintillator was viewed by a 12-cm diameter photomultiplier tube at each end. A position signal was derived from the time difference between the two photomultipliers. The detector arrangement is shown schematically in Fig. 1. The scintillator material used in the cells was BC501.[33] Plastic scintillator veto paddles of 1-mm thickness were placed in front of the forward-angle detectors in order to detect high-energy protons which penetrate the target chamber walls. One of the 12-cm position-sensitive detectors was placed in a vertical orientation so that it subtended a range of angles from in plane at one end to approximately 30° out of plane at the other. Because of difficulties with the efficiency measurements near the ends of the position-sensitive detectors, only the central 60 cm of these detectors were used in the data analysis. For convenience in presentation, the ranges used were divided into five 12-cm wide cells for each position-sensitive detector and are

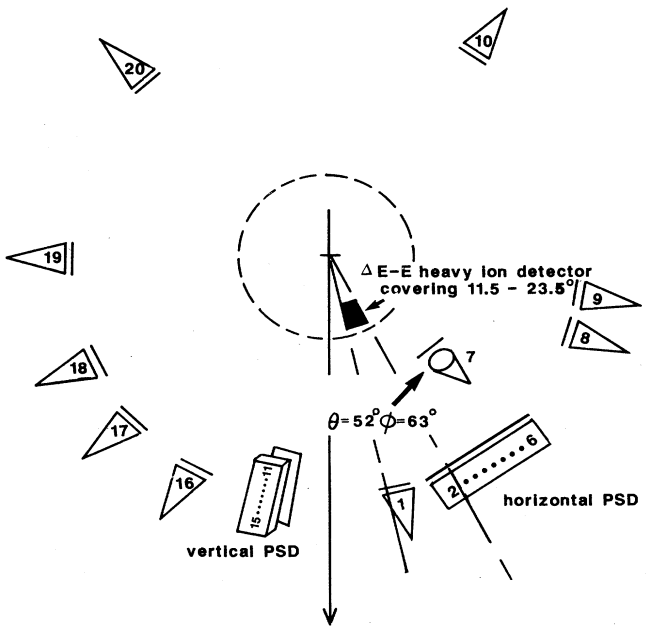

FIG. 1. Detector arrangement used in the experiment.

treated in the remainder of this paper as individual detectors numbered 2–6 for the horizontal and 11–15 for the vertical position sensitive detector. Table I gives the positions of the neutron detectors. Negative values of the angle θ are used to denote detectors on the opposite side of the beam from the heavy-ion detector telescope. The neutron energies were determined by time of flight with respect to the cyclotron rf. The overall time resolution, limited mainly by the beam burst duration, was about 1.5 ns. Thresholds corresponding to neutron energies of 1.5 MeV for the 12-cm diameter detectors and 2.5 MeV for the position-sensitive detectors were set off line on the neutron detector energy signals. Gamma-rays were rejected by pulse-shape discrimination. The spectra have been corrected for random coincidences.

The efficiency of the neutron detectors was checked by measuring coincidences between neutrons and fission fragments from a ^{252}Cf source. The source was mounted flush on the face of a silicon detector at the target position. In addition the Monte Carlo code of Cecil *et al.*[34] was used to calculate the efficiences for neutron energies greater than $\cong$10 MeV. The ^{252}Cf measurements were combined with the predictions of this code to obtain estimates of the neutron flux attenuation due to the target chamber walls and the heavy-ion detector. The low-energy neutron attenuation factors were typically 10–15 percent and have been applied as a correction to the detector efficiencies over the entire neutron energy range up to 80 MeV. For detector 1, which was located directly behind the heavy-ion telescope, the attenuation was approximately 40 percent. Since the neutron attenuation is expected to be smaller for high-energy neutrons, the detection efficiency may be underestimated by as much as the measured attenuation factors for large neutron energies. This results in a significant uncertainty for the spectral shape of detector 1.

III. RESULTS

A. Inclusive fragment distributions

The moments of the measured inclusive fragment distributions as a function of TKE loss are shown in Figs. 2–4. The TKE loss, the velocity, and angle of the target-like fragment (TLF), and the velocity of the PLF were calculated assuming two-body kinematics with the PLF mass taken to be that of the most stable element for the detected PLF charge. (Note that, because the TKE-loss calculation is based on the measured charge of the PLF after light-particle emission has taken place, the resulting TKE losses will be larger than if they were determined before particle emission occurred.) The first and second moments on the PLF charge distribution are shown in Fig. 2. With increasing TKE loss a marked drift toward charges smaller than the projectile charge is evident with a broad distribution extending down to very small Z. The extracted moments of the velocity and angular distributions of the PLF and TLF are shown in Figs. 3 and 4, respectively. The PLF velocities range from slightly less than the beam velocity (5.6 cm/ns) at the smallest TKE losses to approximately 4.5 cm/ns at the largest TKE losses. The PLF angles range from the innermost angle of the detector telescope at the smallest TKE losses to slightly beyond the middle of the detector at the largest TKE losses. The observed PLF angular distribution is strongly influenced by the detector acceptance.

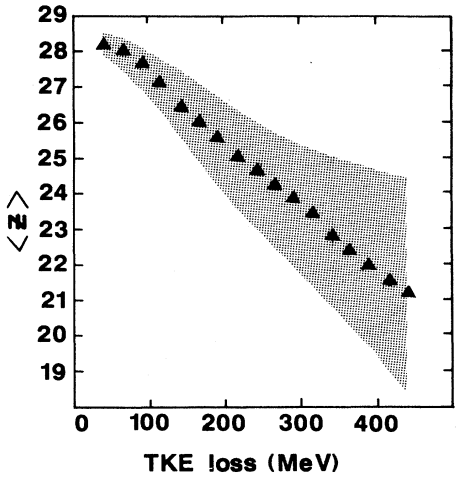

FIG. 2. Average charge as a function of TKE loss of PLF singles events recorded by the heavy-ion detector telescope for $Z \geq 6$. The shaded area surrounding the data points extends to one standard deviation from the average.

B. Neutron spectra—moving source fits

1. Characteristics of the spectra

The energy spectra of neutrons in coincidence with PLF's ($Z \geq 6$) for events with small, intermediate, and large TKE losses are shown in Figs. 5–7. Several features

TABLE I. Neutron detector angles.

Detector number	1	2	3	4	5	6	7	8	9	10
θ	14	22	27	31	36	40	52	70	80	143
Φ	0	0	0	0	0	0	63	0	0	0
Detector number	11	12	13	14	15	16	17	18	19	20
θ	−26	−23	−20	−18	−16	−32	−48	−64	−90	−137
Φ	123	129	137	147	159	0	0	0	0	0

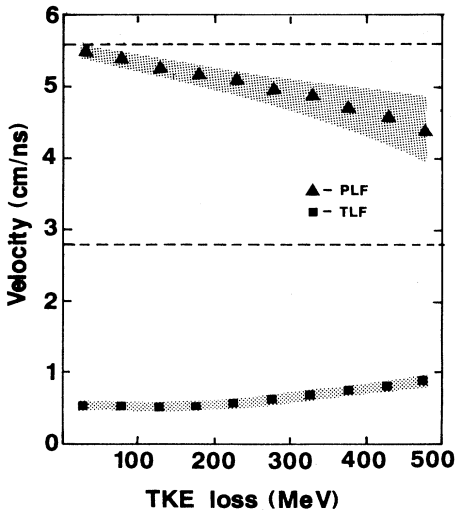

FIG. 3. Average velocities of neutron emission sources as a function of TKE loss determined from the inclusive PLF distributions. Triangles are for the PLF and squares for the TLF. The two horizontal dashed lines are shown at the beam velocity and one half the beam velocity. The shaded areas surrounding the data points extend to one standard deviation from the average values.

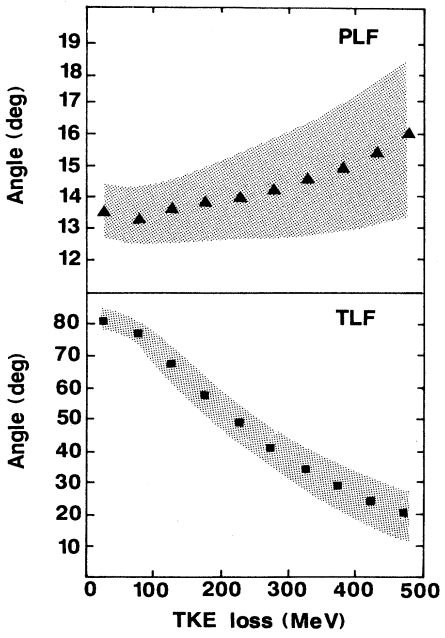

FIG. 4. Average angles of PLF and TLF sources as a function of TKE loss determined from the inclusive fragment distributions. Triangles are for the PLF and squares for the TLF. The shaded areas surrounding the data points extend to one standard deviation from the average values.

of the spectra which are important for our analysis are clearly evident in these figures. First, there is a broad peak, centered at a neutron energy of approximately 20 MeV in the spectra of those detectors which are located at angles near to that of the heavy-ion detector telescope. Neutron detector number 1, for which this peak is the most pronounced, is positioned at $\theta=14°$, directly behind the inner edge of the telescope. These broad peaks result from kinematic focusing of low-energy neutrons emitted from the high-velocity PLF. Second, for large TKE losses, as shown in Figs. 6 and 7, there are noticeable high-energy tails on the forward-angle spectra attributable to nonequilibrium emission. Third, the back-angle spectra have very small high-energy tails and fall relatively steeply with increasing neutron energy, which indicates that for neutron energies less than about 20 MeV these spectra are significantly influenced only by emission from the TLF.

In order to determine the characteristics of the sources of the observed neutron emission we have performed moving source fits to the spectra as a function of TKE loss using 25-MeV-wide TKE-loss bins. Three sources were assumed to be present, corresponding to the TLF, PLF, and a nonequilibrium source. The laboratory spectrum of the ith source was assumed to be of the form

$$\frac{d^2N_i}{dE_n d\Omega} = A_i\sqrt{E_n}\exp-(E_n+\varepsilon_i-2\sqrt{E_n\varepsilon_i}\cos\theta_i)/T_i \ , \tag{1}$$

with θ_i the angle between the direction of travel of the neutron and the ith source, T_i the temperature of the source, and E_n the laboratory neutron energy. Here $\varepsilon_i=\frac{1}{2}m_n v_i^2$ is the laboratory kinetic energy of a neutron which is at rest in the frame of the ith source which moves with velocity v_i. The neutron multiplicity is then given by

$$M_i=2A_i(\pi T_i)^{3/2}/N_{\rm tot} \ , \tag{2}$$

where $N_{\rm tot}$ is the total number of events recorded by the heavy-ion detector. The parameters which can be varied to obtain the best fit to the spectra are A, T, θ, and ε (or the source velocity).

2. *TLF source parameters*

Determination of moving source parameters for the TLF source is simplified by the fact that emission from the TLF dominates the spectra at backward angles. Thus the TLF parameters can be unambiguously determined by fitting these spectra alone. The procedure which produced the most reliable results consisted of first fitting the spectra from those detectors farthest, in angle, from the heavy-ion telescope (detectors 10 and 18–20) with the assumption that they are produced by emission from a single source. The spectra were fitted over a neutron energy range between 3 and 16 MeV. This limited range was chosen to be well above the 1.5-MeV threshold and well below the energies at which any nonequilibrium emission

might be important. The results of these fits are summarized in Table II. Figures 8 and 9 show representative spectra in which the contributions from the TLF source and the PLF and nonequilibrium sources to be discussed in the following sections are shown separately. The results obtained for the velocities and angles of this source are shown in Figs. 10 and 11. The curves indicate the average velocities and angles determined from the

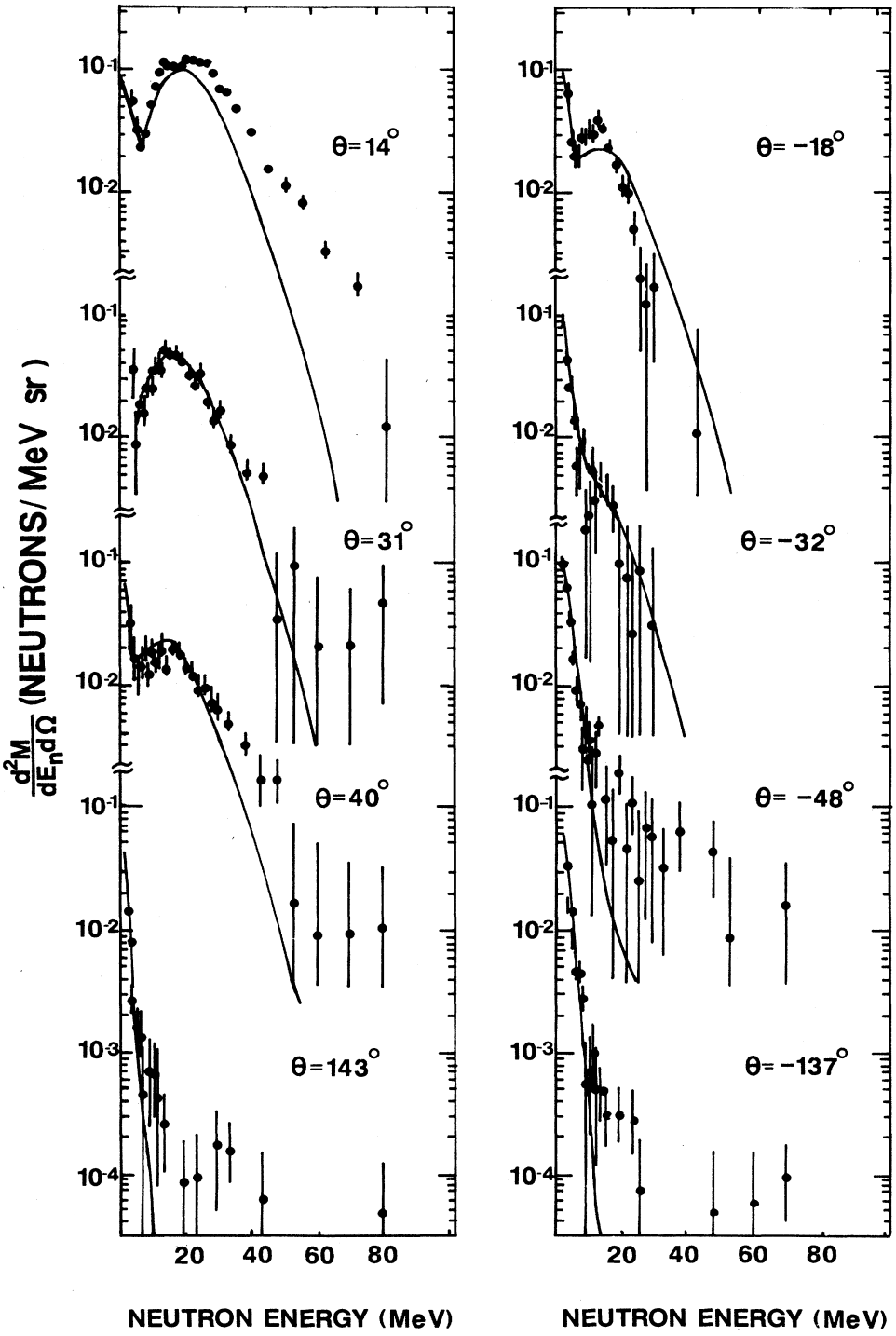

FIG. 5. Representative neutron spectra for TKE losses between 50 and 75 MeV. The left-hand panel shows spectra recorded in detectors on the same side of the beam as the heavy-ion detector telescope. The right-hand panel shows spectra for detectors on the opposite side of the beam. The curves show the results of the moving source fits to the spectra.

analysis of the inclusive PLF distributions (see Figs. 3 and 4). The values obtained by these two independent analyses agree quite close with each other over the entire range of TKE losses from 0 to 450 MeV.

The source emission temperatures and the multiplicities obtained by substituting the best-fit values of A and T into Eq. (2) are shown as a function of TKE loss in Figs. 12 and 13. The values of χ^2 per degree of freedom

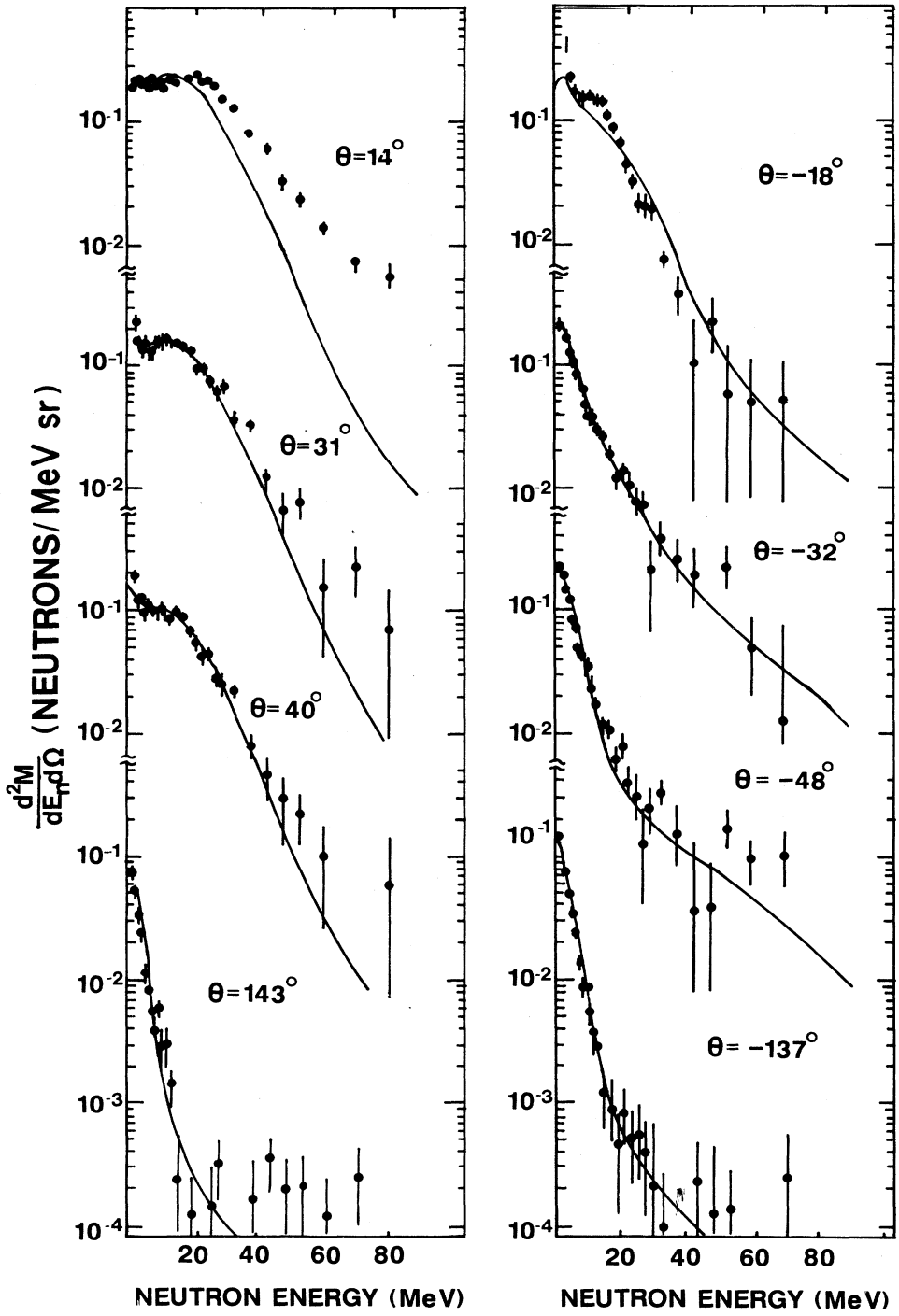

FIG. 6. Same as Fig. 5, but for TKE losses between 275 and 300 MeV. This TKE-loss bin is the smallest for which reliable fits could be made to determine nonequilibrium source parameters.

resulting from these fits range from 1.5 to 5.5. There are no noticeable discrepancies between the data points and the fitted curves shown in Figs. 5–7 for any back-angle detector indicating that Eq. (1) satisfactorily describes the emission of neutrons from the TLF.

3. *PLF parameters for small TKE losses*

Determination of parameters for the PLF and nonequilibrium sources is complicated by the fact that they both contribute to the forward-angle spectra, making it

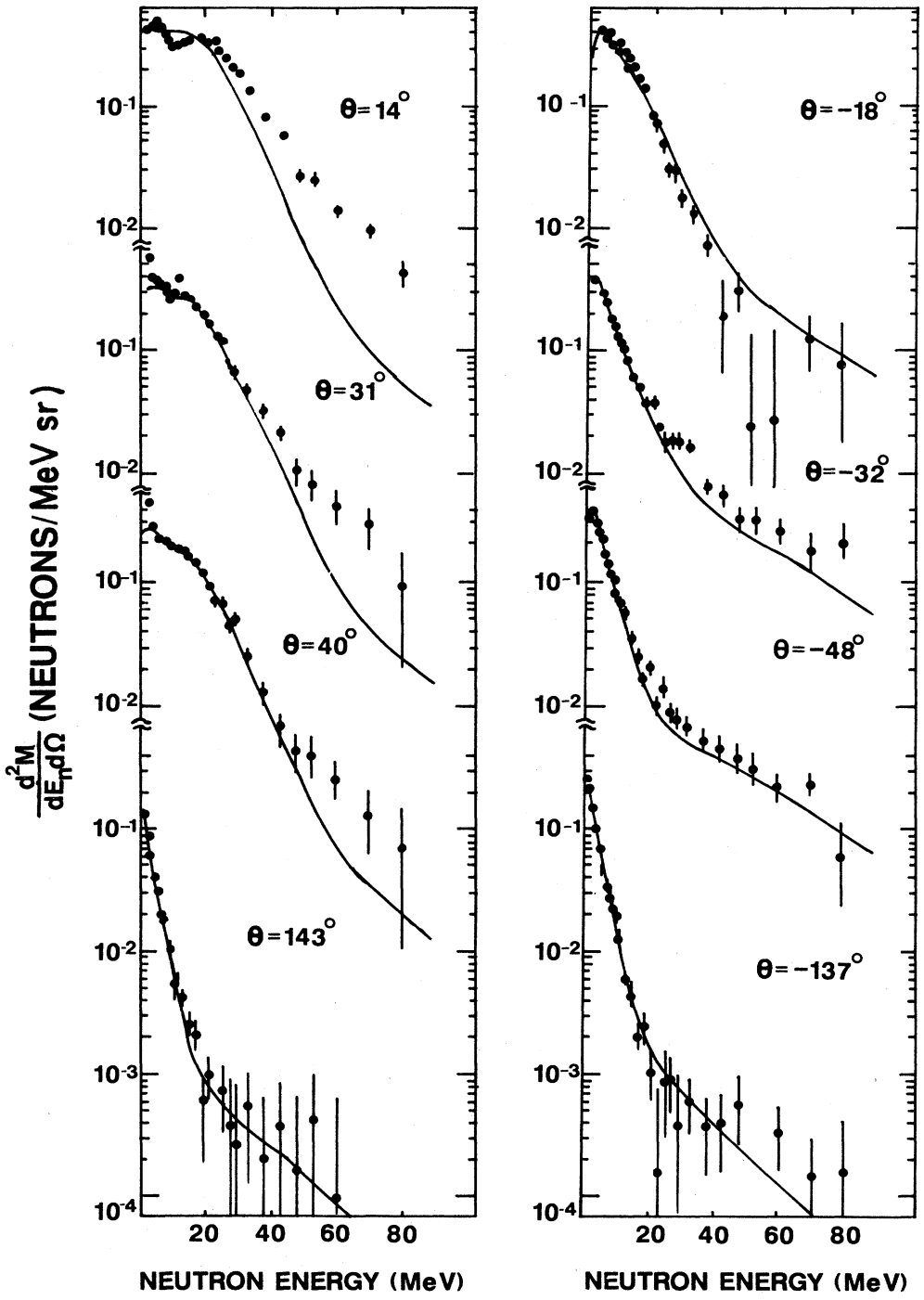

FIG. 7. Same as Fig. 6, but for TKE losses between 400 and 425 MeV.

TABLE II. Parameters for TLF source obtained from moving source fits.

TKE loss (MeV)	χ^2	T (MeV)	V (cm/ns)	θ (deg)	M
0– 25	1.5	1.5±0.1	0.7±0.1	−69.8±14.0	1.7±0.3
25– 50	2.1	1.3±0.1	0.7±0.1	−68.4±13.7	1.6±0.2
50– 75	3.4	1.3±0.1	0.6±0.1	−65.0±13.0	1.4±0.2
75–100	3.0	1.3±0.1	0.6±0.1	−64.9±13.0	2.2±0.3
100–125	2.6	1.6±0.2	0.6±0.1	−62.7±12.5	2.8±0.4
125–150	3.4	1.7±0.2	0.6±0.1	−61.7±12.3	3.3±0.5
150–175	2.7	1.8±0.2	0.6±0.1	−60.9±12.2	3.8±0.6
175–200	2.7	1.6±0.2	0.7±0.1	−70.1±14.0	4.2±0.6
200–225	3.0	2.0±0.2	0.7±0.1	−58.0±11.6	4.9±0.7
225–250	2.7	2.1±0.2	0.6±0.1	−54.6±10.9	5.6±0.8
250–275	2.7	2.2±0.2	0.6±0.1	−51.1±10.2	6.2±0.9
275–300	3.4	2.3±0.2	0.7±0.1	−50.7±10.1	6.9±1.0
300–325	4.0	2.4±0.2	0.7±0.1	−47.3±9.5	7.9±1.2
325–350	3.6	2.5±0.2	0.7±0.1	−49.7±9.9	8.6±1.3
350–375	3.4	2.6±0.3	0.8±0.1	−46.1±9.2	9.5±1.4
375–400	4.2	2.7±0.3	0.8±0.1	−42.8±8.6	10.2±1.5
400–425	5.5	2.8±0.3	0.8±0.1	−40.4±8.1	10.5±1.6
425–450	5.4	3.0±0.3	0.9±0.1	−35.6±7.1	11.1±1.7

difficult to separate the two contributions. However, for TKE losses less than 275 MeV, the high-energy tails of the neutron spectra produced by nonequilibrium emission are so small that they can be ignored. For the smallest TKE losses, therefore, parameters for a PLF source were determined by using only two moving sources, one of whose parameters were fixed at the values determined for the TLF source. The fits were made over the neutron energy range between 10 and 80 MeV. The fits to the spectra of all the detectors were quite good except for the case of detector 1. In this case the predicted and measured spectra agree reasonably well for neutron energies up to approximately 20 MeV (see Figs. 5–7, 14° spectra) but at higher energies the predicted multiplicities are smaller than the measured ones by a factor of 2 or more. We ascribe the discrepancy at the highest neutron energies at least partially to a probable overestimate of the neutron attenuation correction for this detector as discussed in Sec. II. The discrepancies at lower neutron energies (20–30 meV) suggest that the moving source model given by Eq. (1) may not accurately describe the spectrum in detector 1. The apparent excess flux of neutrons reaching detector 1 may arise from emission due to the decay of particle unstable low-lying discrete states in the PLF. If these nonthermal particles are emitted with small relative velocities in the rest frame of the emitting PLF they will all be kinematically focused into the neutron detector directly behind the heavy-ion telescope. For these reasons, detector 1 was excluded from the forward-angle fits. Several different combinations of detectors were used in the fitting procedure as a check to determine if significantly different parameter values result when detector 1 is included. We found that, as long as a set of at least four forward-angle detectors is used, we obtain the same temperatures and multiplicities to within ±10% whether or not the detector set includes detector 1. The final PLF source parameters were obtained using all detectors except number 1 in the fitting procedure.

4. PLF and nonequilibrium source parameters for large TKE losses

For TKE losses larger than 275 MeV, where the high-energy tails due to nonequilibrium emission are significant the PLF and nonequilibrium source parameters were simultaneously determined by fitting the spectra for all detectors except detector 1 using three moving sources, two of which represented the PLF and nonequilibrium sources, respectively, and one of whose parameters were fixed at the values determined for the TLF. This procedure gives satisfactory results except that the resulting nonequilibrium source temperatures and the PLF source angles are highly correlated, giving equally good fits for a wide range of angles and temperatures. To eliminate this effect we made use of the fact that the PLF source angles determined from the fits for small TKE losses were consistently smaller than the average values determined from the inclusive fragment distributions by approximately 2° (see Fig. 11). This consistent discrepancy between the inclusive and exclusive PLF measurements may be attributed to recoil effects. Such effects have been noted in connection with previous neutron and alpha emission measurements.[19,35] Therefore, for the simultaneous determination of PLF and nonequilibrium source parameters at TKE looses larger than 275 MeV the PLF source angles were fixed, for each TKE-loss bin, at an angle 2° smaller than the average angle measured for the inclusive PLF distributions and the other PLF and nonequilibrium source parameters were varied to obtain the best fit. For TKE losses smaller than 275 MeV the statistical uncertainties in the data points comprising the high-energy tails of the spectra are so large that the

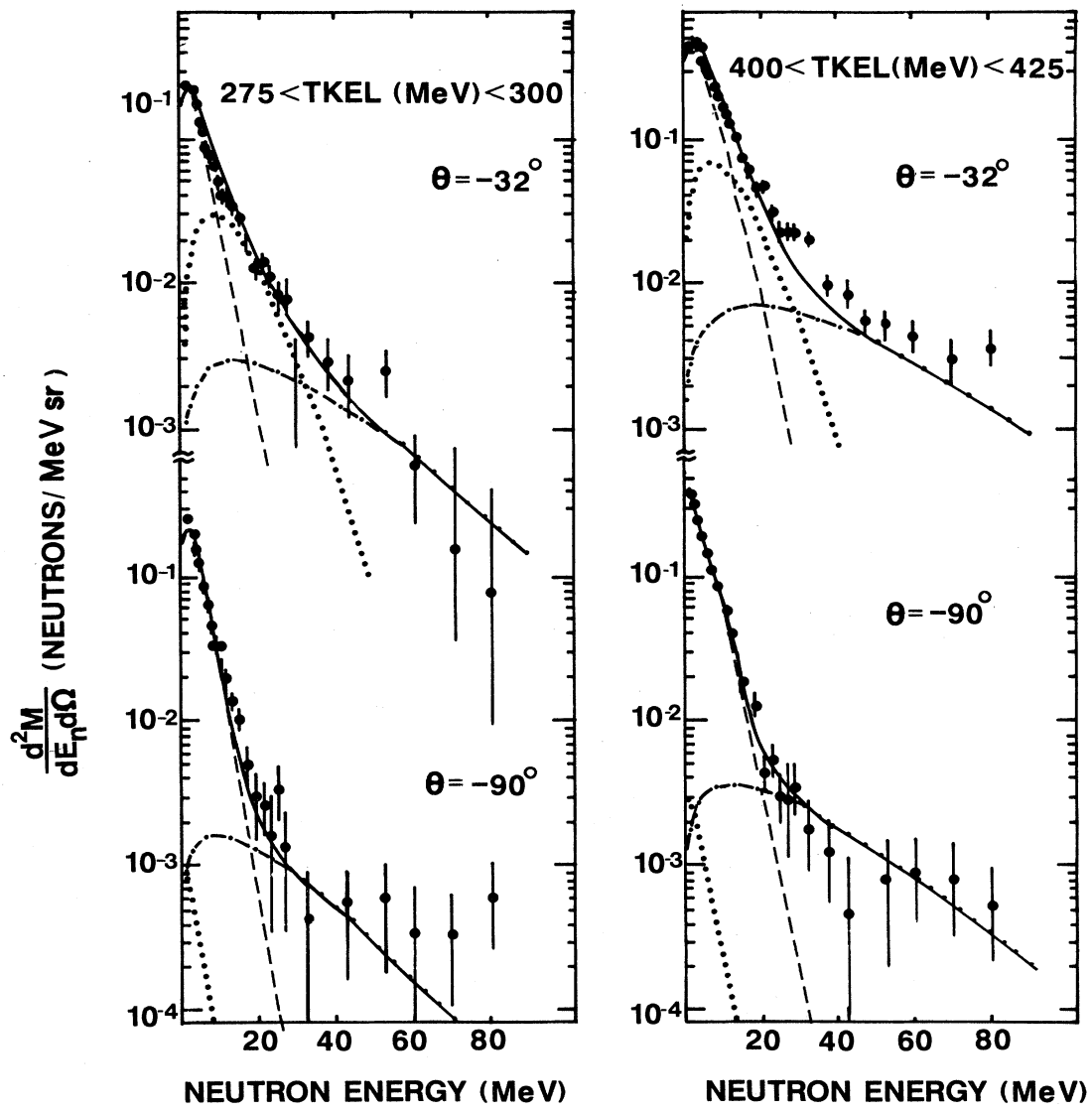

FIG. 8. Neutron spectra for small- and large-angle detectors for TKE-loss bins of 275–300 MeV (left-hand side) and 400–425 MeV (right-hand side). The contributions from the TLF (dashed line), PLF (dotted line), nonequilibrium (dashed-dotted line), and the sum (solid line) are shown superimposed on the spectra.

fitting procedure fails to determine the nonequilibrium source parameters properly. However, reasonable fits can be obtained if the number of nonequilibrium source parameters is reduced. Therefore, since the nonequilibrium source temperature and velocity determined by fitting the spectra over the TKE-loss range from 275 to 450 MeV remain fairly constant at 16 meV and 3.2 cm/ns, respectively, the nonequilibrium source temperature and velocity were fixed at these values and the amplitude of the nonequilibrium source and all of the PLF source parameters were varied to obtain the best fit. Although this procedure gave satisfactory results, the uncertainties in the resulting nonequilibrium source multiplicities increased steadily with decreasing TKE loss. For TKE losses smaller than 100 MeV, the fit results are not improved by inclusion of the nonequilibrium source.

Figure 8 shows several representative spectra for two different TKE-loss bins on which curves representing the contributions of the three sources are superimposed. The curves clearly show the increased multiplicity of the nonequilibrium source for the higher TKE loss.

Three recent reports of nonequilibrium particle emission have indicated a strong preference for in-plane emission.[8,17,18] Our results do not show strong evidence for such an effect. One of our position-sensitive neutron detectors extended to almost 30° above the reaction plane and detector 7 was 63° above the plane, as shown in Table I. A typical fit to this detector is shown in Fig. 9, which

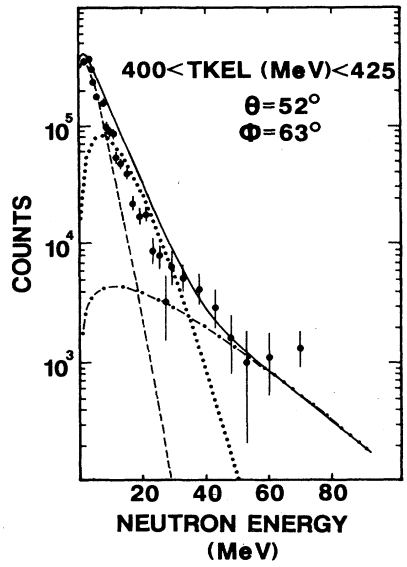

FIG. 9. Three-source fit to neutron detector number 7 which was farthest from the reaction plane. The TKE-loss range is 400–425 MeV.

shows the results of the three-source fit for a TKE loss of 400–425 MeV. Clearly the fit to the high-energy tail does not fall far above the data points as would be expected if there were a strong preference for in-plane emission.

The procedures used to determine the PLF and none-

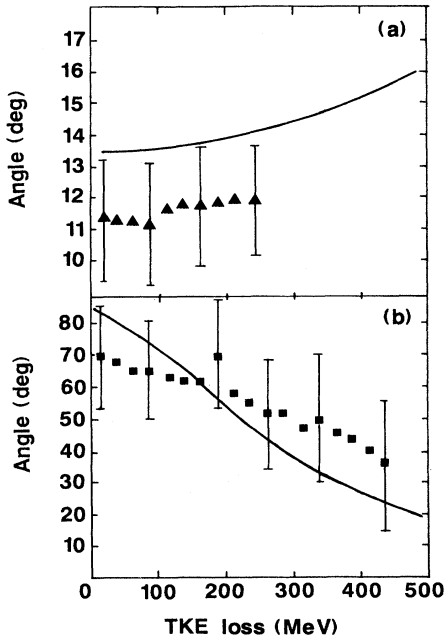

FIG. 11. Angles as a function of TKE loss determined from moving source fits to the neutron energy spectra for (a) and PLF and (b) the TLF sources. The two solid curves superimposed on the data points indicate the angles shown in Fig. 4 which were obtained from the inclusive PLF measurements.

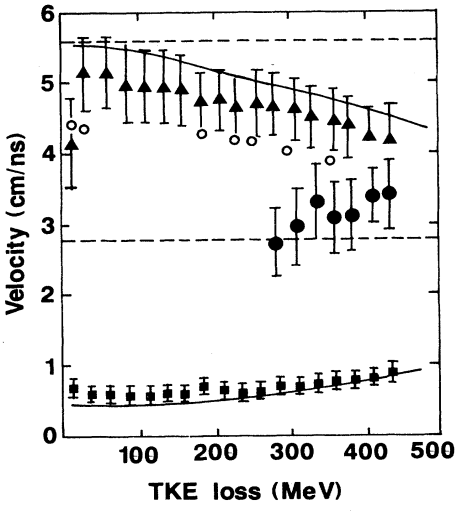

FIG. 10. Velocities of neutron emission sources as a function of TKE loss. Triangles are for the PLF, squares for the TLF, and closed circles for the nonequilibrium source as determined from moving source fits to the neutron energy spectra. The two solid curves superimposed on the data points indicate the velocities shown in Fig. 3 which were obtained from the inclusive PLF measurements. The open circles are the result of TDHF calculations described in the text. The two horizontal dashed lines are shown at the beam velocity and one half the beam velocity.

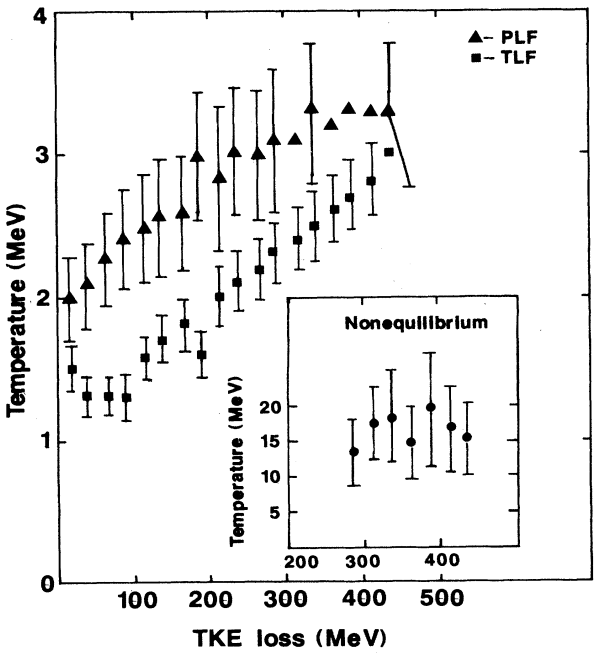

FIG. 12. Source emission temperature for the PLF (triangles), TLF (squares), and nonequilibrium source (circles) resulting from the moving source fits.

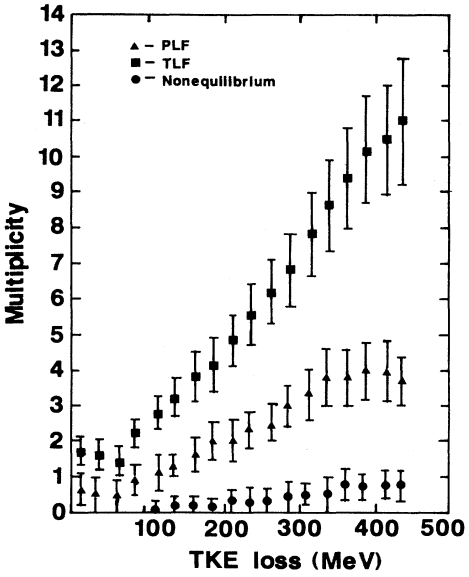

FIG. 13. Same as Fig. 12 but for source multiplicities instead of temperatures.

quilibrium source parameters may then be summaried as follows: Over the TKE loss range from 0 to 100 MeV nonequilibrium emission was found to be negligible and two-source fits were used to determine parameters for the PLF source. Over the TKE-loss range from 100 to 275 MeV three-source fits were used to determine the PLF and nonequilibrium source parameters with all nonequilibrium source parameters fixed except the amplitude. Over the TKE-loss range from 275 to 450 MeV three-source fits were used with the PLF angles fixed at 2° smaller than the average values determined for the inclusive fragment distributions but with all other parameters for both PLF and nonequilibrium sources varied to obtain the best fit.

5. *Discussion of errors*

The uncertainties in the values of each parameter for the TLF and PLF sources are estimated based on the magnitude of the change in the parameter required to double the value of χ^2 resulting from the fit while keeping the other parameters fixed at their optimum values. For the TLF the uncertainty in the multiplicities is approximately $\pm 15\%$ and for the temperatures is estimated to be $\pm 10\%$. The fits were fairly insensitive to the angles; the uncertainty in the angles is estimated to be $\pm 20°$.

The values of χ^2 per degree of freedom resulting from the two- and three-source fits are 2.4 at the smallest TKe losses but increase steadily with increasing TKE loss to greater than 6 for the largest TKE-loss bin. The larger values of χ^2 indicate that neither emission from the PLF nor from the nonequilibrium source is described completely adequately by a single moving source at the large TKE losses. Nevertheless, the uncertainties in the PLF source parameters are essentially the same over the entire range of TKE losses: $\pm 20\%$ for the multiplicities, $\pm 15\%$ for the temperatures, $\pm 10\%$ for the velocities.

Estimating the uncertainties in the nonequilibrium source parameters is difficult because they only affect the high-energy portions of the spectra. We estimated the uncertainties by sequentially rather than simultaneously determining the PLF and nonequilibrium source parameters. PLF source parameters were determined by fitting the spectra over the neutron energy range from 10 to 50 MeV assuming the presence of two moving sources, one of whose parameters was fixed at the TLF source values. Nonequilibrium source parameters were then determined by fitting the high-energy tails of the spectra over the energy range from 30 to 80 MeV assuming the presence of three sources, two of whose parameters were fixed at the TLF and PLF source values, respectively. This procedure tended to minimize the nonequilibrium source multiplicity and velocity and maximize its temperature. Then, to obtain upper estimates for the nonequilibrium source multiplicity and velocity and lower estimates for the temperature, the sequence in which the fits were made to determine PLF and nonequilibrium source parameters was reversed. All fitting procedures used in the analysis gave PLF source parameters that agree with each other within $\pm 10\%$. The nonequilibrium source multiplicities determined by all the procedures attempted in our anaysis agree with each other to within $\pm 20\%$ for large TKE losses but diverge from each other as the TKE loss decreases. The temperatures and velocities remain essentially constant over the entire TKE loss range for all fitting procedures but are different for each fitting procedure, with the temperatures ranging from 10 to 25 MeV and the velocities ranging from about 2.5 to 3.5 cm/ns. The inability of a single moving source to account for all features of the spectra is especially evident in the determination of the source direction. The angle is very poorly determined by all procedure, but averages about $-20°$.

IV. DISCUSSION

The results of these fits are shown in Figs. 10–13. The velocities and angles are shown in Figs. 10 and 11 with superimposed curves representing the average values determined by analysis of the inclusive PLF distributions (see Figs. 3 and 4). The source temperatures and multiplicities are shown in Figs. 12 and 13. The nonequilibrium source velocity and temperature are shown in Figs. 10 and 12 only for the TKE loss range over which these parameters were fitted, namely from 275 to 450 MeV. Similarly, the nonequilibrium source multiplicity is shown in Fig. 13 only over the range from 100 to 450 MeV and the PLF angle is shown in Fig. 11 only over the range from 0 to 275 MeV. The results of the two- and three-source fits are also summarized in Table III. As in the case of Figs. 10–13, the extracted parameters are shown in the table only for the TKE loss ranges over which they were fitted. The multiplicity of the nonequilibrium source increases with increasing TKE loss but its temperature and velocity are constant within uncertainties, averaging 16 MeV and 3.2 cm/ns, respectively, over the TKE loss range

TABLE III. Parameters for PLF and nonequilibrium sources determined from moving source fits.

TKE loss		PLF source T	v	θ		Nonequilibrium source T	v	θ	
(MeV)	χ^2	(MeV)	(cm/ns)	(deg)	M	(MeV)	(cm/ns)	(deg)	M
0– 25	2.4	2.0±0.3	4.2±0.4	11.5±2.3	0.7±0.1				
25– 50	2.4	2.1±0.3	5.1±0.5	11.3±2.3	0.6±0.1				
50– 75	2.4	2.3±0.3	5.1±0.5	11.3±2.3	0.6±0.1				
75–100	2.6	2.4±0.4	4.9±0.5	11.3±2.3	0.9±0.2				
100–125	2.6	2.5±0.4	4.9±0.5	11.5±2.3	1.1±0.2				0.1±0.1
125–150	2.6	2.6±0.4	4.9±0.5	11.6±2.3	1.3±0.3				0.2±0.1
150–175	2.4	2.6±0.4	4.9±0.5	11.7±2.3	1.6±0.3				0.2±0.1
175–200	2.9	3.0±0.4	4.8±0.5	11.8±2.4	2.0±0.4				0.1±0.1
200–225	3.1	2.8±0.4	4.8±0.5	12.0±2.4	2.0±0.4				0.3±0.1
225–250	2.9	3.0±0.4	4.7±0.5	12.0±2.4	2.3±0.5				0.3±0.1
250–275	3.0	3.0±0.5	4.7±0.5	12.1±2.4	2.5±0.5				0.3±0.1
275–300	3.4	3.1±0.5	4.6±0.5		3.0±0.6	13±7	2.7±0.4	−20±10	0.4±0.1
300–325	3.6	3.1±0.5	4.6±0.5		3.4±0.7	17±9	3.0±0.4	−20±10	0.5±0.1
325–350	4.3	3.3±0.5	4.5±0.4		3.7±0.7	19±9	3.3±0.5	−20±10	0.5±0.1
350–375	4.6	3.2±0.5	4.5±0.4		3.9±0.8	15±7	3.1±0.5	−20±10	0.8±0.2
375–400	4.7	3.3±0.5	4.4±0.4		4.1±0.8	19±0	3.1±0.5	−20±10	0.7±0.1
400–425	5.8	3.3±0.5	4.2±0.4		4.0±0.8	16±8	3.4±0.5	−20±10	0.8±0.2
425–450	6.4	3.3±0.5	4.2±0.4		3.8±0.8	15±8	3.4±0.5	−20±10	0.8±0.2

from 275 to 450 MeV. The nonequilibrium source temperatures are large but are consistent with tempratures reported for products of similar reactions[1–21] if the large uncertainties are taken into account.

As in the case of the TLF source, the PLF source temperature and multiplicity increase with increasing TKE loss as shown in Figs. 12 and 13. It is interesting to note that the extracted temperature of the PLF source is larger than that of the TLF. In fact, at small TKE loss it is seen that

$$T_{\mathrm{PLF}}/T_{\mathrm{TLF}} \cong (A_{\mathrm{TLF}}/A_{\mathrm{PLF}})^{0.5}$$

as expected for equal division of the available excitation energy between PLF and TLF. The extracted temperatures are approximately equal, corresponding to a fully thermalized energy division, only at the largest TKE loss. This result is in contrast to other results in which temperatures extracted by similar moving source fits have indicated that thermalization occurs already at relatively small TKE loss[36–40] but is consistent with more recent analyses in which the excitation energy division is extracted by other means.[41–45] The difficulties of extracting the excitation energy from the fitted temperatures has recently been pointed out by Wile *et al.*[46] Alternatively, the measured TLF and PLF neutron multiplicities may be combined with the final PLF charge distributions determined from the inclusive fragment distributions to determine the division of excitation energy between the fragments during the collision. However, in order to determine this division unambiguously these data must be combined with information about the final PLF masses.[41] These results will be presented in a forthcoming publication.

As discussed in Sec. I, the variation of the nonequilibrium source velocity with PLF velocity may provide a means to choose between models which picture the nonequilibrium emission as resulting from the quasifree scattering between individual nucleons of the target and projectile on the one hand or from a time-dependent external field on the other. As shown in Fig. 10, for the TKE loss range over which the nonequilibrium source velocity could be reliably determined using moving source fits, the nonequilibrium source velocity is approximately one-half the beam velocity. For comparison the open circles indicate the average velocity of the nonequilibrium neutrons for nucleon emission induced by the time dependence of the mean field of the projectile as calculated in time-dependent Hartree Fock.[28] These calculations are done in two steps. First TDHF calculations are used to determine the TKE loss as a function of impact parameter. Then the model is used to calculate the source velocities as a function of impact parameter using the formula

$$\langle v \rangle_{\mathrm{source}} = \frac{\int_{-\infty}^{+\infty} v_{\mathrm{PLF}}(t) P(t) dT}{\int_{-\infty}^{+\infty} P(t) dt} , \tag{3}$$

where $v_{\mathrm{PLF}}(t)$ is the velocity of the PLF during its collision with the target and $P(t)$ is the probability of emission of a neutron at time t. The source velocity calculated in this way closely follows the final PLF velocity extracted from the inclusive measurements (solid curve) and moving source fits (triangles). It is slightly smaller than the final PLF velocity for all TKE losses, indicating that most of the emission takes place while the PLF is in contact with the target. (We note that the TDHF calculations are shown for the true TKE loss calculated according to the primary reaction partners. Therefore, for comparison the experimental velocity points should be shifted

to smaller TKE losses to take into account the overestimate of the actual TKE loss due to the effects of particle evaporation. This shift is approximately 100 MeV at the largest TKE loss.) We have chosen to compare our results with this model as representative of mean-field models. Other models[24–26] which similarly assume nonequilibrium emission to occur via isotropic emission in the projectile rest frame along either the incoming or outgoing trajectories would also predict an apparent nonequilibrium source velocity which would closely follow that of the final PLF. An analogous low-velocity source would be expected for nonequilibrium emission from the target. The observed nonequilibrium source velocities are smaller than the velocities predicted by these types of models for all TKE losses and appear inconsistent with such an emission process. Instead the observations indicate a nonequilibrium component which arises from the overlap of nearly equal target and projectile contributions, such as in a hot-spot[20,21] or nucleon-nucleon collision models,[20,22,23] giving rise to apparent emission from the nucleon-nucleon center-of-mass frame. In these models the increasing nonequilibrium neutron multiplicity with increasing TKE loss shown in Fig. 13 would be expected due to the increasing overlap of target and projectile at small impact parameters.

V. SUMMARY

We have analyzed our results for neutron emission from products of strongly damped reactions of ^{58}Ni+^{165}Ho at 930 MeV in terms of moving sources in order to extract emission parameters for PLF, TLF, and nonequilibrium neutron sources. As a function of TKE-loss the nonequilibrium multiplicity is observed to increase. The extracted temperatures of the PLF and TLF emission sources also increase with increasing TKE loss with the PLF source temperatures exceeding the TLF source temperatures. The ratio of the temperatures of the two fragments suggests an equal division of the available excitation energy between target and projectile with thermalization approached only at the largest TKE losses.

At large TKE losses the nonequilibrium source temperature and velocity are observed to be independent of TKE loss. The velocity of the nonequilibrium emission source is found to be constant at approximately one-half the beam velocity which is significantly different from the final velocities of the reaction partners. This result supports models of nonequilibrium emission in which emission is isotropic in the rest frame of roughly equal target and projectile overlap such as models in which individual nucleon-nucleon collisions dominate rather than models which assume isotropic emission from either the target or projectile fragments.

ACKNOWLEDGMENTS

We wish to thank Dr. Dean and M. R. Strayer for helpful discussions and to thank them and A. S. Umar for sharing their results prior to publication. This work is supported by the U.S. Department of Energy, under Contract Nos. DE-AC05-84OR21400 with Martin Marietta Energy Systems, Inc. and DE-FG05-84ER40162 with Georgie State University.

[1]E. Holub, D. Hilscher, G. Ingold, U. Jahnke, H. Orf, and H. Rossner, Phys. Rev. C **28**, 252 (1983).

[2]H. Machner, D. Protic, G. Riepe, H. G. Bohlen, and H. Fuchs, Phys. Rev. C **31**, 443 (1985).

[3]G. Caskey, A. Galonsky, B. Remington, M. B. Tsang, C. K. Gelbke, A. Kiss, F. Deak, Z. Seres, J. J. Kolata, J. Hinnefeld, and J. Kasagi, Phys. Rev. C **31**, 1597 (1985).

[4]G. A. Petitt, A. Gavron, J. R. Beene, B. Cheynis, R. L. Ferguson, F. E. Obenshain, F. Plasil, G. R. Young, M. Jääskeläinen, D. G. Sarantites, and C. F. Maguire, Phys. Rev. C **32**, 1572 (1985).

[5]G. Caskey, A. Galonsky, B. Remington, F. Deak, A. Kiss, and Z. Seres, Phys. Rev. C **34**, 506 (1986).

[6]B. A. Remington, G. Caskey, A. Galonsky, C. K. Gelbke, L. Heilbronn, J. Heltsley, M. B. Tsang, F. Deak, A. Kiss, Z. Seres, J. Kasagi, and J. J. Kolata, Phys. Rev. C **34**, 1685 (1986).

[7]E. Holub, D. Hilscher, G. Ingold, U. Jahnke, H. Orf, H. Rossner, W. P. Zank, W. U. Schröder, H. Gemmeke, K. Keller, L. Lassen, and W. Lücking, Phys. Rev. C **33**, 143 (1986).

[8]W. P. Zank, D. Hilscher, G. Ingold, U. Jahnke, M. Lehmann, and H. Rossner, Phys. Rev. C **33**, 519 (1986).

[9]W. Rösch, W. Cassing, H. Gemmeke, R. Gentner, K. Keller, L. Lassen, W. Lücking, A. Richter, R. Schreck, and G. Schrieder, Phys. Lett. B **197**, 19 (1987).

[10]H. J. Rabe, K. D. Hildebrand, U. Lynen, W. F. J. Müller, H. Sann, H. Stelzer, W. Trautmann, R. Trockel, R. Wada, J. Pochodzalla, E. Eckert, P. Kreutz, A. Kuhmichel, N. Brummund, R. Glasow, K. H. Kampert, R. Santo, and D. Pelte, Phys. Lett. B **196**, 439 (1987).

[11]F. Deak, A. Kiss, Z. Seres, G. Caskey, A. Galonsky, C. K. Gelbke, B. Remington, M. B. Tsang, and J. J. Kolata, Nucl. Phys. **A464**, 133 (1987).

[12]Z. Chen, C. K. Gelbke, J. Pochodzalla, C. B. Chitwood, D. J. Fields, W. G. Gong, W. G. Lynch, and M. B. Tsang, Nucl. Phys. **A473**, 564 (1987).

[13]A. Gavron, A. Gayer, J. Boissevain, H. C. Britt, T. C. Awes, J. R. Beene, B. Cheynis, D. Drain, R. L. Ferguson, F. E. Obenshain, F. Plasil, G. R. Young, G. A. Petitt, and C. Butler, Phys. Rev. C **35**, 579 (1987).

[14]D. Hilscher, H. Rossner, A. Gamp, U. Jahnke, B. Cheynis, B. Chambon, D. Drain, C. Pastor, A. Giorni, C. Morand, A. Dauchy, P. Stassi, and G. Petitt, Phys. Rev. C **36**, 208 (1987).

[15]W. Rösch, A. Richter, G. Schrieder, R. Gentner, K. Keller, L. Lassen, W. Lücking, R. Schreck, W. Cassing, and H. Gem meke, Phys. Lett. B **197**, 19 (1987).

[16]C. Bloch, W. Benenson, A. I. Galonsky, E. Kashy, J. Heltsley, L. Heilbronn, M. Lowe, B. Remington, D. Morrisey, and J. Kasagi, Phys. Rev. C **36**, 203 (1987).

[17]C. Bloch, W. Benenson, A. I. Galonsky, E. Kashy, J. Heltsley, L. Heilbronn, M. Lowe, R. J. Radtke, B. Remington, J. Kasagi, and D. J. Morrisey, Phys. Rev. C **37**, 2469 (1988).

[18]M. B. Tsang, C. B. Chitwood, D. J. Fields, C. K. Gelbke, D. R. Klesch, and W. G. Lynch, Phys. Rev. Lett. **52**, 1967 (1984).
[19]I. Tserruya, A. Breskin, R. Chechik, Z. Fraenkel, S. Wald, N. Zwang, R. Bock, M. Dakowski, A. Gobbi, H. Sann, R. Bass, G. Kreyling, R. Renfordt, K. Stelzer, and U. Arlt, Phys. Rev. C **26**, 2509 (1982).
[20]T. C. Awes, S. Saini, G. Poggi, C. K. Gelbke, D. Cha, R. Legrain, and G. D. Westfall, Phys. Rev. C **25**, 2361 (1982).
[21]R. Weiner and M. Weström, Nucl. Phys. **A286**, 282 (1977).
[22]William R. Friedman, Phys. Rev. C **29**, 139 (1984).
[23]J. Randup and R. Vandenbosch, Nucl. Phys. **A474**, 219 (1987).
[24]W. Cassing and W. Norenberg, Nucl. Phys. **A401**, 467 (1983).
[25]J. P. Bondorf, J. N. De, G. Fai, A. O. T. Karvinen, B. Jakobsen, and J. Randrup, Nucl. Phys. **A333**, 285 (1980).
[26]S. Leray, G. La Rana, C. Ngo, M. Barranco, M. Pi, and X. Vinas, Z. Phys. A **320**, 383 (1985).
[27]A. S. Umar, M. R. Strayer, D. J. Ernst, and K. R. S. Devi, Phys. Rev. C **30**, 1934 (1984); A. S. Umar, M. R. Strayer, and D. J. Ernst, Phys. Lett. **140B**, 290 (1984); Phys. Rev. Lett. **55**, 584 (1985).
[28]D. J. Dean, A. S. Umar, and M. R. Strayer, submitted to Phys. Rev. C.
[29]G. D. Harp, J. M. Miller, and B. J. Berne, Phys. Rev. **165**, 1166 (1968); G. D. Harp and J. M. Miller, Phys. Rev. C **3**, 1847 (1971).
[30]M. Blann, Phys. Rev. C **23**, 205 (1981).
[31]B. A. Remington, M. Blann, A. Galonsky, L. Heilbronn, F. Deak, A. Kiss, and Z. Seres, Phys. Rev. C **38**, 1746 (1988).
[32]A. Iwamoto, Phys. Rev. C **35**, 984 (1987).
[33]Bicron Corporation, 12345 Kinsman Rd., Newbury, Ohio 44065.
[34]R. A. Cecil, B. D. Anderson, and R. Madey, Nucl. Instrum. Methods **161**, 439 (1979).
[35]A. Gavron, J. R. Beene, B. Cheynis, R. L. Ferguson, F. E. Obenshain, F. Plasil, G. R. Young, G. A. Petitt, and C. F. Maguire, Phys. Rev. C **27**, 450 (1983); A. Gavron, J. R. Beene, B. Cheynis, R. L. Ferguson, F. E. Obenshain, F. Plasil, G. R. Young, G. A. Petitt, K. Geoffroy-Young, M. Jääskeläinen, D. G. Sarantites, and C. F. Maguire, *ibid.* **24**, 2048 (1981).
[36]B. Tamain, R. Chechik, H. Fuchs, F. Hanappe, M. Morjean, C. Ngo, J. Peter, M. Dakowski, B. Lucas, C. Mazur, M. Ribrag, and C. Signarbieux, Nucl. Phys. **A330**, 253 (1979).
[37]Y. Eyal, A. Gavron, I. Tserruya, Z. Fraenkel, Y. Eisen, S. Wald, R. Bass, G. R. Gould, G. Kreyling, R. Renfordt, K. Stelzer, R. Zitzmann, A. Gobbi, U. Lynen, H. Stelzer, I. Rode, and R. Bock, Phys. Rev. Lett. **41**, 625 (1978).
[38]B. Cauvin, R. C. Jared, P. Russo, R. P. Schmitt, R. Babinet, and L. G. Moretto, Nucl. Phys. **A301**, 511 (1978).
[39]R. Babinet, B. Cauvin, J. Girard, H. Nifenecker, B. Gatty, D. Guerreau, M. Lefort, and X. Tarrago, Nucl. Phys. **A296**, 160 (1978).
[40]D. Hilscher, J. R. Birkelund, A. D. Hoover, W. U. Schröder, W. W. Wilcke, J. R. Huizenga, A. C. Mignerey, K. L. Wolf, H. F. Breuer, and V. E. Viola, Phys. Rev. **20**, 576 (1979).
[41]T. Awes, R. L. Ferguson, R. Novotny, F. E. Obenshain, F. Plasil, S. Pontoppidan, V. Rauch, G. R. Young, and H. Sann, Phys. Rev. Lett. **52**, 251 (1984).
[42]D. R. Benton, H. Breur, F. Khazaie, K. Kwiatkowski, V. E. Viola, S. Bradley, A. C. Mignerey, and A. P. Weston-Dawkes, Phys. Rev. C **38**, 1027 (1988).
[43]R. Vandenbosch, A. Lazzarini, D. Leach, D.-K. Lock, A. Ray, and A. Seamster, Phys. Rev. Lett. **52**, 1964 (1984).
[44]L. G. Sobotka, G. J. Wozniak, R. J. McDonald, M. A. McMahan, R. J. Charity, L. G. Moretto, Z. H. Liu, F. S. Stephens, R. M. Diamond, M. A. Deleplanque, and A. J. Pacheco, Phys. Lett. B **175**, 27 (1986).
[45]H. Solbach, H. Freieslaben, P. Braun-Munzinger, W. F. W. Schneider, D. Schüll, B. Kohlmeyer, M. Marinescu, and F. Pulhofer, Phys. Lett. **153B**, 386 (1985); H. Sohlbach, H. Freieslaben, W. F. W. Schneider, D. Schüll, P. Braun-Munzinger, B. Kohlmeyer, M. Marinescu, and F. Pulhofer, Nucl. Phys. **A467**, 349 (1987); H. Solbach, H. Freiesleben, W. F. W. Schneider, D. Schüll, B. Kohlmeyer, M. Marinescu, and F. Pulhofer, Z. Phys. A **328**, 205 (1987).
[46]J. L. Wile, W. U. Schröder, J. R. Huizenga, and D. Hilscher, Phys. Rev. C **35**, 1608 (1987).